

## Radiative electron capture in relativistic atomic collisions

Akira Ichihara, Toshizo Shirai, and Jörg Eichler\*

*Tokai Research Establishment, Japan Atomic Energy Research Institute,  
Tokai-mura, Ibaraki 319-11, Japan*

(Received 5 October 1993)

Radiative electron capture (REC) from a low- $Z$  target atom into a bare high- $Z$  projectile is described in the impulse approximation for the momentum distribution of the captured electron in the initial target state. Otherwise the treatment is rigorous by using exact relativistic Coulomb wave functions for the bound and continuum projectile states. As an application of the computer program, photon spectra and differential cross sections have been calculated for 295-MeV/u  $U^{92+} + N$  collisions. The angular distributions for  $K$ -shell REC as well as for  $L$ -shell REC show pronounced deviations from  $\sin^2 \theta$ . Cross sections for radiative recombination with capture into the  $K$  shell and into the  $L$  subshells are presented for projectile charges between 20 and 100 and for energies between 100 MeV/u and 2 GeV/u.

PACS number(s): 34.70.+e

### I. INTRODUCTION

With the currently developing possibilities to accelerate highly stripped high- $Z$  ions to relativistic velocities, new frontiers are opened up in atomic structure as well as in atomic collision physics. Atomic structure studies of high- $Z$  few-electron atoms such as hydrogenlike or heliumlike gold and uranium atoms [1] may serve as a testing ground for quantum electrodynamics in the non-perturbative domain of strong fields. The starting point for experimental investigations of this kind will always be the production of the desired species in a specific quantum state. This, in turn, requires an understanding of the basic atomic processes. For a recent review, see Ref. [2].

One of the basic processes occurring in nonrelativistic as well as in relativistic collisions is electron transfer accompanied by the simultaneous emission of a photon. This process is usually denoted as radiative electron capture (REC). Under certain conditions, the cross section for radiative electron capture can be much larger than the cross section for nonradiative electron capture. The reason is the following. In the nonrelativistic energy regime, the nonradiative capture cross section falls off with increasing projectile velocity  $v$  as  $v^{-12}$  (or as  $v^{-11}$  in second order). This rapid decrease is mainly caused by the requirement that a given momentum component in the initial electronic wave function has to find its counterpart in the final momentum wave function displaced by the momentum  $m_e v$  of an electron traveling with the speed of the projectile. With increasing displacement, the overlap of the tails of the two momentum distributions will rapidly decrease. If, however, the electron transfer is accompanied by the emission of a photon, the severe requirement of momentum matching will be re-

laxed, so that the cross section for REC falls off as  $v^{-5}$  for high nonrelativistic projectile velocities.

For free electrons, capture cannot occur at all without the emission of photons, owing to energy and momentum conservation. This means, qualitatively, that electrons loosely bound in low- $Z$  target atoms or in outer shells are more likely to be captured *with* photon emission than without. Hence for low- $Z$  target atoms at high projectile energies, the REC cross section exceeds the cross section for (nonradiative) Coulomb capture. We will focus our attention on radiative electron capture from low- $Z$  targets into high- $Z$  projectiles. Experimentally, the process of REC has been identified by Raisbeck and Yiou [3], and by Schnopper *et al.* [4], and since that time has been extensively studied both experimentally and theoretically [5–12]. More recently, the interest has been extended to the relativistic energy regime [13–15].

The theoretical treatments of radiative electron capture in relativistic collisions have followed two different lines. (a) In a direct formulation, approximate distorted-wave methods have been applied to a direct evaluation of the transition amplitude [15]. (b) Existing results for the inverse reaction, namely the photoelectric effect, have been used to estimate REC cross sections and to reproduce experimental data [13,14]. The underlying picture is the following [3,7]: A loosely bound target electron may be regarded as approximately free in a high-energy collision. In this limit, REC is identical with radiative recombination (RR) in which an electron initially moving with the momentum  $-\mathbf{p}_0$  in the projectile frame is captured into a bound state with the simultaneous emission of a photon. Radiative recombination is the inverse of the photoelectric effect and can be calculated by detailed balancing. The effect of electron binding in the target just gives rise to a momentum spread around  $-\mathbf{p}_0$  which is usually taken into account by the Compton profile, see, e.g., [2,7].

Both groups of publications are not yet fully satisfactory. Regarding (a), we have to be aware of the fact that, to leading order, REC, in contrast to Coulomb capture, is subject to selection rules which are likely to be violated

---

\*Permanent address: Bereich Theoretische Physik, Hahn-Meitner-Institut Berlin, 14109 Berlin, Germany, and Fachbereich Physik, Freie Universität Berlin, 14195 Berlin, Germany.

by approximate wave functions, so that significant spurious contributions may appear [2]. The approach (b), in our opinion, represents the most practical way; however, formulas for differential cross sections for the photoelectric effect are available in an  $\alpha Z$  expansion not suitable for high- $Z$  projectiles. Exact numerical results are also available but not always for differential cross sections and for the systems required. Therefore “similar” systems have been used for comparison with experimental data [13].

In the present publication, “dedicated” rigorous calculations for the photoelectric effect and for radiative recombination are combined with an exact convolution with the momentum distribution of the electron in its initial target state to calculate differential REC cross sections. This amounts to an impulse approximation for the electron initially bound in the low- $Z$  target.

In Sec. II, we provide the theoretical framework for our treatment and in Sec. III give applications to the double-differential cross section, to the angle-dependent single-differential cross section, and to radiative recombination for the  $K$  and  $L$  shells. In Sec. IV, we add some concluding remarks. Natural units  $\hbar = m_e = c = 1$  are used unless explicitly stated otherwise.

## II. THEORETICAL DESCRIPTION

### A. REC from radiative recombination

In order to avoid the problems of a “direct” formulation addressed in the Introduction, we focus our attention on the accurate description of a Coulomb-distorted electron-projectile system and include the (low- $Z$ ) target in the description only insofar as it gives rise to a momentum distribution of quasifree electrons. In this description [2,3,7,13], we refer all quantities to the projectile coordinate frame and visualize the process as radiative recombination of free electrons moving with respect to the projectile with momentum  $\mathbf{q}'$ , which results from Lorentz transforming the momentum  $\mathbf{q} = (\mathbf{q}_\perp, q_z)$  of the electron in its initial state is given by the momentum distribution  $\rho(q)$  within the target atom. In all cases, we assume that  $q \ll \gamma v$ . Although the electrons are treated kinematically as free, we require the energy conservation in the form

$$\omega' + E_f = \gamma(E_i - vq_z), \quad (2.1)$$

where  $\gamma = 1/\sqrt{1-v^2}$ ,  $E_i$  and  $E_f$  are the energies (including the rest mass) of the initial and final atomic states,  $\omega'$  is the photon energy in the projectile system, and the right-hand side of Eq. (2.1) results from the Lorentz transformation of the energy-momentum four-vector. In terms of the RR cross section, the cross section for radiative electron capture is written as

$$\frac{d^2\sigma_{\text{REC}}}{d\omega' d\Omega'} = \int d^3q \frac{d\sigma_{\text{RR}}(\mathbf{q}')}{d\Omega'} \rho(\mathbf{q}) \delta(\omega' + E_f - \gamma E_i + \gamma v q_z), \quad (2.2)$$

where  $\Omega'$  denotes the photon angle in the projectile system.

The calculation proceeds in the following steps: (1) The photoelectric differential cross section in the projectile frame  $\sigma_{\text{ph}}$  is calculated and (2) converted into the cross section  $\sigma_{\text{RR}}$  for radiative recombination. (3) The resulting cross section is folded with the momentum spread due to the electronic momentum distribution in the initial target state. (4) The frequencies  $\omega'$ , the angles  $\Omega'$ , and the cross sections are Lorentz transformed into the laboratory frame. The following subsections deal with these steps.

### B. The photoelectric cross section

The photoelectric effect has been treated since the early days of quantum mechanics, and approximate formulas for the differential cross section in the case of relativistic electrons are available to various degrees of sophistication [16–19]. However, the existing tabulations for exactly evaluated cross sections [19] are not very suitable for use with Eq. (2.2) which requires differential cross sections on a sufficiently dense mesh. We have therefore developed an independent computer code in which from the outset we confine ourselves to unpolarized photons and assume that no polarization measurement is performed for the electrons. Exact bound and continuum wave functions for an extended nucleus are used [20].

In this subsection, we omit the primes which indicate that the quantities are defined in the projectile frame. Then, for a given photon energy  $\omega$  and binding energy  $\epsilon_b$  of the electron in the bound initial state  $b$ , the final electron energy  $E$  (including the rest mass) is determined by

$$E = \omega + 1 - \epsilon_b, \quad (2.3)$$

and the differential cross section for a single electron is [17]

$$\frac{d\sigma_{\text{ph}}}{d\Omega} = \frac{\alpha}{4\omega} \frac{1}{2j_b + 1} \sum_{\mu_b} \sum_{m_s} |M_{\mathbf{p},b}(m_s, \lambda_+, \mu_b)|^2, \quad (2.4)$$

where we have averaged over the  $(2j_b + 1)$  angular momentum projections  $\mu_b$  in the bound state and have summed over the spin projections  $m_s = \pm \frac{1}{2}$  of the emitted electron. Furthermore, we have averaged over the circular polarizations  $\lambda_+ = 1$  and  $\lambda_- = -1$  of the incoming photon. Because of the summation over all other angular momentum projections,  $\mu_b$  and  $m_s$ , this is equivalent to taking one photon polarization, e.g.,  $\lambda_+ = 1$ , only. The quantity  $\alpha$  denotes the fine-structure constant.

The transition matrix element is

$$M_{\mathbf{p},b}(m_s, \lambda_+, \mu_b) = \int \psi_{\mathbf{p},m_s}^\dagger(\mathbf{r}) \alpha \cdot \hat{\mathbf{u}}_+ e^{i\mathbf{k}\cdot\mathbf{r}} \psi_{j_b,\mu_b}(\mathbf{r}) d^3r, \quad (2.5)$$

where

$$\psi_{\mathbf{p}, m_s}(\mathbf{r}) = 4\pi \sum_{\kappa, \mu} i^l e^{i\Delta_\kappa} \langle l, \mu - m_s, \frac{1}{2}, m_s | j, \mu \rangle \times Y_{l, \mu - m_s}^*(\theta, 0) \begin{pmatrix} g_\kappa(r) \chi_\kappa^\mu \\ i f_\kappa(r) \chi_{-\kappa}^\mu \end{pmatrix}, \quad (2.6)$$

is the partial-wave expansion of the wave function describing the relativistic electron emitted with asymptotic momentum  $\mathbf{p}$  ( $p^2 = E^2 - 1$ ,  $p_z = p \cos \theta$ ) and spin projection  $m_s$  with respect to the  $z$  axis. The summation extends over the relativistic quantum number  $\kappa = \pm(j + \frac{1}{2})$  and the angular momentum projection  $\mu$ . Associated with  $\kappa$  are the orbital angular momenta  $l$  and  $l'$  of the upper and lower components, respectively. The  $\chi_\kappa^\mu$  are the usual [2,21] normalized two-component spin-angular functions, and the  $g_\kappa(r)$  and  $f_\kappa(r)$  are the (real) radial continuum wave functions. They are normalized on the energy scale, and their asymptotic behavior is given by

$$g_\kappa \simeq \frac{1}{r} \sqrt{\frac{E+1}{\pi p}} \cos(kr + \sigma_\kappa), \quad (2.7)$$

$$f_\kappa \simeq -\frac{1}{r} \sqrt{\frac{E-1}{\pi p}} \sin(kr + \sigma_\kappa).$$

In the limit of a point nucleus, the Coulomb phase shift is

$$\sigma_\kappa = \Delta_\kappa + \eta \ln(2pr)$$

$$\Delta_\kappa = \frac{1}{2} \arg \left( \frac{-\kappa + i\eta/E}{s + i\eta} \right) - \arg \Gamma(s + i\eta) - \frac{1}{2} \pi s \quad (2.8)$$

$$\eta = \frac{\alpha Z E}{p}, \quad s = \sqrt{\kappa^2 - (\alpha Z)^2}.$$

$$F_{\mu_b}^+(L, \kappa) = \left[ A_L(j_b \mu_b j; l_b' l) \int_0^\infty g_\kappa(r) j_L(kr) f_b(r) r^2 dr - A_L(j_b \mu_b j; l_b l) \int_0^\infty f_\kappa(r) j_L(kr) g_b(r) r^2 dr \right], \quad (2.11)$$

and

$$A_L(j_b \mu_b j; l_1 l_2) = (2L+1) \sqrt{\frac{2l_1+1}{2l_2+1}} \langle l_1, \mu_b + \frac{1}{2}, \frac{1}{2}, -\frac{1}{2} | j_b, \mu_b \rangle \langle l_2, \mu_b + \frac{1}{2}, \frac{1}{2}, \frac{1}{2} | j, \mu_b + 1 \rangle \times \langle l_1, \mu_b + \frac{1}{2}, L, 0 | l_2, \mu_b + \frac{1}{2} \rangle \langle l_1, 0, L, 0 | l_2, 0 \rangle. \quad (2.12)$$

It is not difficult to carry the analytical reduction further [17,19] by squaring the matrix element Eq. (2.10) and by expanding the resulting products of spherical harmonics. In this way, additional summations are introduced. Since, however, our aim is numerical evaluation, we do not perform this step. Hence Eq. (2.4) with Eq. (2.10) represent our final result for the atomic photoeffect.

We may also quantize the spin of the emitted electron in the direction of its motion. In this way, the continuum electron wave function is expressed in terms of the Wigner rotation matrices. In the calculation of the differential cross section, one then obtains an expansion in terms of Legendre polynomials. After checking the numerical identity of the two representations, we have abandoned the latter because it requires longer computing times.

Equations (2.7) and (2.8) serve to clarify our normalization and phase conventions. In our actual calculations, we use the generalization for an extended nucleus given by Müller *et al.* [20]. The Clebsch-Gordan coefficient  $\langle \dots | \dots \rangle$  in Eq. (2.6) mediates a projection onto the definite spin component  $m_s$  in the  $z$  direction and onto a definite orbital angular momentum  $l$  entering into the directional dependence expressed by  $Y_{l, \mu - m_s}^*(\theta, 0)$ . Owing to the axial symmetry, an azimuthal dependence does not occur.

Returning to Eq. (2.5), the bound-state wave function is written as

$$\psi_{j_b, \mu_b}(\mathbf{r}) = \begin{pmatrix} g_b(r) \chi_{\kappa_b}^{\mu_b} \\ i f_b(r) \chi_{-\kappa_b}^{\mu_b} \end{pmatrix}. \quad (2.9)$$

Here, we use again wave functions for an extended nucleus [20]. If we now insert the Rayleigh expansion of the photon plane wave and perform the spinor algebra, we arrive at integrals over three spherical harmonics which can be expressed by Clebsch-Gordan coefficients. Collecting the results, we obtain

$$M_{\mathbf{p}, b}(m_s, \lambda_+, \mu_b) = 4\pi\sqrt{2} \sum_{L=0}^{\infty} \sum_{\kappa} i^{L+1-l} e^{i\Delta_\kappa} \times \langle l, \mu_b + 1 - m_s, \frac{1}{2}, m_s | j, \mu_b + 1 \rangle \times F_{\mu_b}^+(L, \kappa) Y_{l, \mu_b + 1 - m_s}(\theta, 0), \quad (2.10)$$

where

The summations occurring in Eq. (2.10) are limited by the selection rules embodied in the Clebsch-Gordan coefficients. In particular, if the electron is initially bound in a  $1s_{1/2}$  state, a rather small number of terms contributes. Most of the published calculations have been performed for this case, usually taking into account screening corrections which are needed for the photoelectric effect in neutral atoms. However, if one wants to use existing tabulations to derive REC cross sections for *bare* projectiles, one has to eliminate these screening corrections [14].

### C. The cross section for radiative recombination

Once we have computed the cross section  $\sigma_{\text{ph}}(\omega', \theta')$  of the photoelectric effect in the projectile frame (we reintroduce primed quantities), it is a simple matter to write

down the cross section  $\sigma_{\text{RR}}(E', \theta')$  for radiative recombination. This is the cross section for capturing a free electron of energy  $E'$  into a bound atomic state (binding energy  $\epsilon$ ) with the simultaneous emission of a photon of energy  $\omega'$ . Since according to Eq. (2.3),  $\omega' = E' - 1 + \epsilon$ , we may use  $E'$  as well as  $\omega'$  to characterize the process. We now choose the direction of the incoming electron as the  $z$  direction, so that  $\theta'$  is the emission angle of the photon.

By the principle of detailed balance, the cross section for radiative recombination is written as

$$\frac{d^2\sigma_{\text{RR}}(E', \theta')}{dE' d\Omega'_{\text{ph}}} = (2j_b + 1) \frac{\omega'^2}{q'^2} \frac{d^2\sigma_{\text{ph}}(E', \theta')}{dE' d\Omega'_{\text{el}}}. \quad (2.13)$$

Here, the factor  $(2j_b + 1)$  turns the averaging of Eq. (2.4) into a summation while the factor  $\omega'^2/q'^2$  replaces the phase-space factor of the outgoing electron by that of the emitted photon.

In applications to relativistic ion-atom collisions, the  $z$  direction is usually defined as the direction of the projectile motion. This is opposite to the direction of the electron momentum as seen from the projectile. Hence for REC, the angle  $\theta'$  of the photoelectric effect or of the radiative recombination has to be replaced by  $\pi - \theta'$ , or  $\cos \theta'$  is replaced by  $-\cos \theta'$ .

#### D. The REC cross section in the projectile frame

In relativistic electron capture, the velocity of the captured electron is essentially determined by the velocity  $-\mathbf{v}$  of the target atom with respect to the projectile. However, an electron bound in the target (which is assumed to have a low charge  $Z_T \ll Z_P$ ) has a momentum distribution  $\rho(\mathbf{q})$ , so that there is a momentum spread around the momentum  $-\mathbf{p}_0 = -2\mathbf{v}$ .

If we assume a spherically averaged distribution for a single electron (averaging over a complete principal shell  $n$ ), the nonrelativistic hydrogenic momentum distribution is given by

$$\rho(q) = \frac{1}{n^2} \sum_l \sum_m |\tilde{\psi}_{nlm}(\mathbf{q})|^2 = \frac{8Q_n^5}{\pi^2 (q^2 + Q_n^2)^4}, \quad (2.14)$$

where  $\tilde{\psi}_{nlm}(\mathbf{q})$  is the Fourier transform of the electronic

$$\frac{d^2\sigma_{\text{REC}}(\omega', \theta')}{d\omega' d\Omega'} = \frac{1}{2\pi} \frac{d^2\sigma_{\text{REC}}(\omega', \theta')}{d\omega' d\cos \theta'} = \frac{1}{2\pi} \int d^2q_{\perp} \int dq_z \int d\cos \bar{\theta} \frac{d^2\sigma_{\text{RR}}(\mathbf{q}', \bar{\theta})}{d\omega' d\cos \bar{\theta}} \left| \frac{\partial \cos \bar{\theta}}{\partial \cos \theta'} \right| \rho(q) \delta(\omega' - \omega'_0 + \gamma v q_z) \times \delta(\cos \bar{\theta} - \cos \theta'_q \cos \theta' - \sin \theta'_q \sin \theta' \cos \phi'_q). \quad (2.17)$$

Here,  $\phi'_q$  is measured with respect to  $\phi' = 0$  chosen to define the  $x$  axis, and

$$\omega'_0 = \gamma E_i - E_f \quad (2.18)$$

is the resonance energy.

With the aid of the delta functions, the integrations

wave function in the state  $\{nlm\}$  and

$$Q_n = \frac{\alpha Z_T}{n}. \quad (2.15)$$

The momentum distribution Eq. (2.14) has a maximum at  $q = 0$  and a width determined by  $Q_n$ : the distribution gets more and more peaked around  $q = 0$ , the lower  $Z_T$  and the higher  $n$ . For an atomic multielectron target, it is more realistic to use the Fourier transforms of Hartree-Fock wave functions as tabulated by Clementi and Roetti [22]. In all our results presented in Sec. III, we use momentum distributions obtained in this way.

Since the electron momentum within the target has a component  $q_{\perp}$  transverse to the beam direction, the momentum seen from the projectile deviates slightly from the  $z$  direction (defined by the beam) and the corresponding angular distribution will be tilted by this amount. For the rather low-energy collision of 197-MeV/u Xe on Be [13], we estimate a deviation from the  $z$  direction by  $\arctan(Q_1/v\gamma) \simeq 4.3^\circ$ , while for higher energies the angle will be less.

For a given electron momentum  $\mathbf{q}$  in the target, the Lorentz-transformed momentum  $\mathbf{q}'$  in the projectile forms the axis of an axially symmetric photon angular distribution. If we denote the polar and azimuthal angle of the photon with respect to  $\mathbf{q}'$  as  $\bar{\theta}$  and  $\bar{\phi}$ , a given direction  $\theta', \phi' = 0$  in the projectile frame will receive contributions from various axes  $\mathbf{q}' = (\theta'_q, \phi'_q)$  and, associated with them, from corresponding angles  $\bar{\theta}$  and  $\bar{\phi}$ . Let us consider the spherical triangle composed of the pole  $P_0 = (\theta = 0)$ , of the point  $P_{\gamma} = (\theta', \phi' = 0)$  giving the direction of the emitted photon, and of the point  $P_q = (\theta'_q, \phi'_q)$  giving the direction of the electron momentum  $\mathbf{q}'$ . The sides in this triangle are  $s_0 = \bar{\theta}$ ,  $s_{\gamma} = \theta'_q$ , and  $s_q = \theta'$ . Knowing the angle  $a_0 = \phi'_q$  at the pole, we can express the opposite side  $s_0 = \bar{\theta}$  by the law of cosines as

$$\cos \bar{\theta} = \cos \theta'_q \cos \theta' + \sin \theta'_q \sin \theta' \cos \phi'_q. \quad (2.16)$$

In this way, we may eliminate the angle  $\bar{\theta}$  by which the photon is emitted with respect to the direction  $\mathbf{q}'$ .

We thus get a generalization of Eq. (2.2) which takes into account the deviations of the electron momenta  $\mathbf{q}'$  from the beam axis and integrates over their contributions. The differential REC cross section in the projectile frame is accordingly

over  $\bar{\theta}$  and  $q_z$  can be carried out to give

$$\frac{d^2\sigma_{\text{REC}}(\omega', \theta')}{d\omega' d\Omega'} = \frac{1}{2\pi\gamma v} \int d^2q_{\perp} \frac{d^2\sigma_{\text{RR}}(\mathbf{q}', \bar{\theta})}{d\omega' d\cos \bar{\theta}} \times \left| \frac{\partial \cos \bar{\theta}}{\partial \cos \theta'} \right| \rho(q). \quad (2.19)$$

Besides the relations Eqs. (2.14), (2.15), and (2.16) we use the abbreviations

$$q' = \sqrt{\gamma^2(E - vq \cos \theta_q)^2 - 1}, \quad (2.20)$$

$$E^2 = q^2 + 1 = q_{\perp}^2 + \left(\frac{\omega'_0 - \omega'}{\gamma v}\right)^2 + 1.$$

Furthermore, from the energy-conserving delta function,

$$\cos \theta_q = \frac{\omega'_0 - \omega'}{\gamma v q}, \quad (2.21)$$

and from the Lorentz transformation,

$$\sin \theta'_q = \frac{q}{q'} \sin \theta_q, \quad (2.22)$$

$$\cos \theta'_q = \frac{\gamma}{q'} (q \cos \theta_q - v \sqrt{q^2 + 1}).$$

In the limiting case  $q_{\perp} \ll q' \simeq v$ , so that the axis of the angular distribution coincides with the  $z$  axis, we have  $\sin \theta'_q = 0$ ,  $\cos \theta'_q = -1$ , and  $|\partial \cos \theta' / \partial \cos \theta| = 1$ . We then get the usual result, Eq. (2.2). The cross section has a peak at  $q = 0$  or at the resonance energy  $\omega'_0$  given by Eq. (2.18). The Doppler width is characterized by  $Q_n$  as defined in Eq. (2.15). The target momentum distribution here enters the cross section simply as the momentum profile [7].

### E. Transformation to the laboratory frame

Experimentally, REC cross sections are measured in the laboratory system as a function of the photon frequency  $\omega$  and/or the emission angle  $\theta$ . We then have to substitute for  $\omega'$  and  $\cos \theta'$  their values expressed in terms of  $\omega$  and  $\cos \theta$  using the relations [2]

$$\omega' = \gamma \omega (1 - v \cos \theta) \quad (2.23)$$

$$\cos \theta' = \frac{\cos \theta - v}{1 - v \cos \theta}.$$

If we are interested in the angular distribution at a fixed frequency, say at the resonance frequency  $\omega'_0$ , in the projectile system or in the complete integral over the resonance line, we obtain the laboratory angular distribution by multiplying with the ratio

$$\frac{d\Omega'}{d\Omega} = \frac{1}{\gamma^2(1 - v \cos \theta)^2} \quad (2.24)$$

of the differential solid angles, so that the desired single-differential cross section becomes

$$\frac{d\sigma_{\text{REC}}(\theta)}{d\Omega} = \frac{d\sigma_{\text{REC}}(\theta')}{d\Omega'} \frac{d\Omega'}{d\Omega}. \quad (2.25)$$

If the emission angle of the photon as well as its energy is measured at the same time, the double-differential cross

section is needed. We then have to evaluate the Jacobian for the transformation  $\omega', \Omega' \rightarrow \omega, \Omega$ . Owing to Eq. (2.23), we have  $\partial \cos \theta' / \partial \omega = 0$ , so that the Jacobian factorizes in the form

$$\frac{\partial(\omega', \Omega')}{\partial(\omega, \Omega)} = \frac{d\omega'}{d\omega} \frac{d \cos \theta'}{d \cos \theta}, \quad (2.26)$$

and the double-differential cross section is given by

$$\frac{d^2 \sigma_{\text{REC}}(\omega, \Omega)}{d\omega d\Omega} = \frac{1}{\gamma(1 - v \cos \theta)} \frac{d^2 \sigma_{\text{REC}}(\omega', \Omega')}{d\omega' d\Omega'}. \quad (2.27)$$

By inserting Eqs. (2.4) and (2.13) into Eq. (2.17) and using the transformations given here, we can calculate the REC cross sections appropriate to various experimentally given situations.

### F. Numerical evaluation

While evaluating REC cross sections, we will need several numerical calculations. The photoelectric cross section Eq. (2.4) is transformed into the RR cross section using Eq. (2.13). The radial functions for the bound and continuum states in Eq. (2.5) can be calculated numerically by solving the radial Dirac equation [20]. In order to avoid the truncation error of the transition matrix elements, a sufficient number of partial waves in the continuum state should be taken into account [17]. After several test calculations of photoelectric cross sections for the  $K$ ,  $L_1$ ,  $L_2$ , and  $L_3$  states, we confirmed that at least the first two digits of the differential cross sections evaluated in our computer code agreed with those of Alling and Johnson [23]. For the collisions of 197-MeV/u  $\text{Xe}^{54+}$  on Be and 295 MeV/u  $\text{U}^{92+}$  on N considered in this paper, we considered all partial waves with  $|\kappa| \leq 10$ . The differential cross section was calculated from  $0^\circ$  to  $180^\circ$  with the interval of  $15^\circ$  to obtain a smooth curve of angular distribution by spline fitting.

The double-differential cross section of REC given by Eq. (2.19) for a single electron in the projectile frame can be evaluated using numerical integration of the RR cross section over  $q_{\perp}$  accompanied by the momentum distribution  $\rho(q)$  of the target electrons. The integration has been carried out in the neighborhood of  $q = 0$ , because  $\rho(q)$  decreases to zero quickly with the increase of  $q$ . We used more than 100 mesh points for each  $q$  and  $\phi$ .

After the double-differential cross section (photon spectrum) Eq. (2.19) for the single electron is obtained, the angle-differential cross section given in Eq. (2.25) for the fixed laboratory angle  $\theta$  is calculated by integrating the right-hand side of Eq. (2.27) over  $\omega$ . The integration should be carried out from the peak of the photon spectrum Eq. (2.18) to both ends with the appropriate interval  $d\omega$  (we chose  $d\omega$  in the range  $1.0 \leq \omega \leq 5.0$  keV) until the converged value is obtained. Then the evaluated cross section is multiplied by the occupation number of electrons in the target state. The final angular distribution for REC is determined by summing up the cross sections from every target state.

### III. RESULTS AND DISCUSSION

With the procedure outlined in Sec. II and the associated computer program, it is possible to evaluate any desired REC cross section for capture into an arbitrary projectile state. As long as the target charge is small compared to the projectile charge, so that the impulse approximation is justified, the calculated results can be expected to be very accurate.

As an illustration, we present various angle-differential cross sections, and for radiative recombination with capture into the  $K$  and  $L$  shells provide the charge and energy dependence between 100 MeV/u and 2 GeV/u.

#### A. Differential cross sections

Anholt *et al.* [13] measured the absolute values of the angle-differential cross section for the  $K$ -shell REC ( $K$ -REC) of 197-MeV/u  $\text{Xe}^{54+}$  incident on Be. As a case study, we have applied the present treatment to this collision system.

The double-differential cross section (photon spectrum) was first calculated with two types of momentum distribution function defined by the hydrogenic wave function and the approximate Roothaan-Hartree-Fock (RHF) wave function (see Sec. IID). The RHF function comprises “double- $\zeta$ ” Slater-type orbitals (DZ-STO’s) given by Clementi and Roetti [22]. Figure 1 shows the result at a fixed laboratory angle  $90^\circ$ , where the angle-differential cross section takes a maximum value. In the figure the spectra depicted with solid and dashed lines are obtained using the RHF and hydrogenic momentum

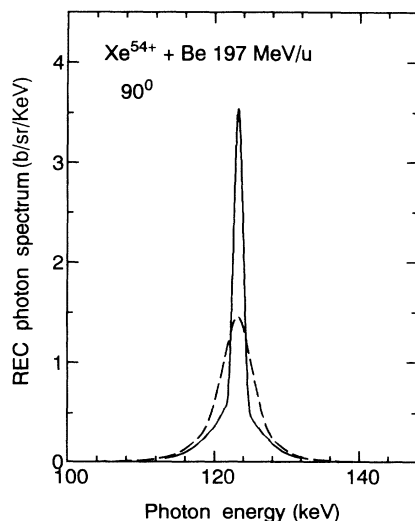


FIG. 1. Calculated  $K$ -REC photon spectrum in b/sr keV for 197-MeV/u  $\text{Xe}^{54+}$  on Be atoms for the laboratory photon angle  $90^\circ$ . Solid line : calculated with the approximate RHF wave functions by DZ-STO’s [22] for the target atom; dashed line: calculated with the hydrogenic momentum distribution for the target atom. All partial waves with  $|\kappa| \leq 10$  have been taken into account in the calculation of the photoelectric cross section.

distribution functions, respectively. Each spectrum is peaked at the resonance photon energy  $\omega'_0$  of 123 keV given by Eq. (2.18). As is considered in Sec. IID, there appears a difference in the line shape. This difference comes from the fact that owing to the screening effect, the RHF momentum distribution is narrow in spread and about twice in maximum value at  $q = 0$  compared with the hydrogenic momentum distribution function. In the present calculation, it turns out that the momentum distribution of target electrons changes the double-differential cross section, but leaves the angle-differential and total cross sections almost unchanged.

The angle-differential  $K$ -REC cross section is shown in Fig. 2 in comparison with the measurement of Anholt *et al.* [13]. The values of the cross section are reduced by a factor of 0.8 for normalization at  $90^\circ$ . This excess of about 20% of the theoretical results over the experimental data is less than the systematic deviation in a recent observation by Stöhlker *et al.* [24]. Aside from the overall normalization, the experimental angular dependence is well represented by our theory. The total  $K$ -REC cross section is predicted to be 81.9 b.

Figure 3 illustrates the calculated photon spectrum at a fixed laboratory observation angle of  $132^\circ$  for the 295-MeV/u  $\text{U}^{92+} + \text{N}$  collision. The photon spectrum calculated with the hydrogenic momentum distribution is also shown by the dashed line. As in Fig. 1, the photon lines for the hydrogenic momentum distribution are broader. A measurement was made by Stöhlker *et al.* [25] for the  $\text{N}_2$  target. Our results based on atomic RHF wave functions give very good agreement with the ex-

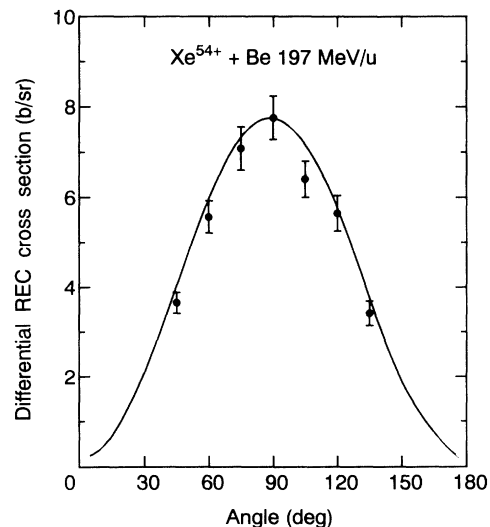


FIG. 2. Differential  $K$ -REC cross section in b/sr for 197-MeV  $\text{Xe}^{54+}$  on Be as a function of the laboratory angle. Measured values are from [13]. In addition to the statistical error, there may be a systematic uncertainty of  $\pm 20\%$ . The solid curve represents the calculated results (this work) multiplied with a normalization factor of 0.8. The approximate RHF wave functions by DZ-STO’s [22] have been used for the target atom. All partial waves with  $|\kappa| \leq 10$  have been taken into account in the calculation of the photoelectric cross section.

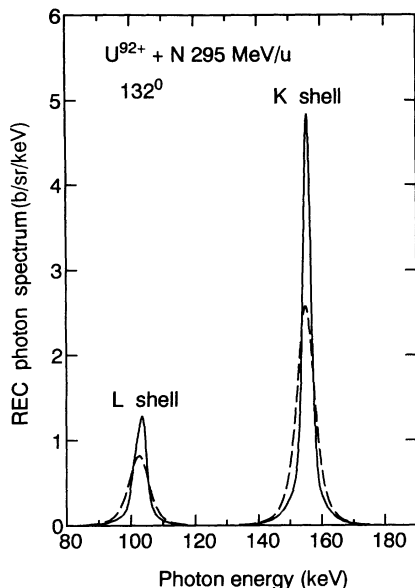


FIG. 3. Calculated REC photon spectrum in b/sr keV for 295-MeV/u  $U^{92+}$  on N atoms for the laboratory photon angle  $132^\circ$ . For the  $L$  shell, the contributions of the subshells are added. Solid line : calculated with the approximate RHF wave functions by DZ-STO's [22] for the target atom; dashed line: calculated with the hydrogenic momentum distribution for the target atom. All partial waves with  $|\kappa| \leq 10$  have been taken into account in the calculation of the photoelectric cross section.

perimentally observed ratio between the peak heights of the  $K$ -REC and  $L$ -REC lines after applying an efficiency correction [26] to the original data (Fig. 1 of [25]). The angle-differential cross sections into  $K$  and  $L$  shells are predicted to be 21.0 and 7.38 b/sr, respectively, at  $132^\circ$ .

Figure 4 gives the differential REC cross sections for capture into the  $K$  and  $L$  shells of the projectile. It is known that in the theoretical description of nonrelativistic REC, the photon angular distribution shows a simple  $\sin^2 \theta$  dependence in the laboratory system [10]. However, both distributions of the present calculation exhibit deviations from a  $\sin^2 \theta$  distribution. The total  $K$ - and  $L$ -REC cross sections are predicted to be 423 and 128 b, respectively.

In order to describe the relativistic effect of REC, the contributions from spin-flip and non-spin-flip transitions to  $K$ -REC are indicated in Fig. 5. At forward (and backward) directions with respect to the electron momentum (which may slightly deviate from the beam direction because of the transverse momentum spread in the target) photon emission is forbidden in a nonrelativistic theory [2], since photon angular momentum  $\pm 1$  cannot be created from axially symmetric electron wave functions. Only the relativistic coupling of the electron spin giving rise to spin flip can lead to a nonzero cross section. From Fig. 5 it is clearly seen that the deviation from a  $\sin^2 \theta$  behavior mainly comes from the spin-flip transition.

The cross section for  $L$ -REC is shown in more detail in Fig. 6, where REC into the individual subshells  $L_1$ ,

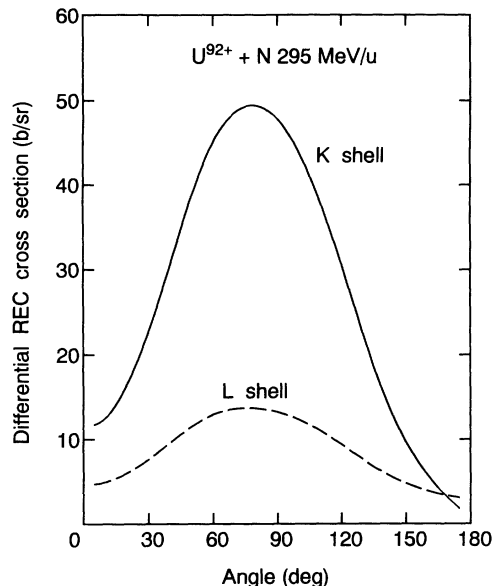


FIG. 4. Calculated differential  $K$ -shell and  $L$ -shell REC cross sections for 295-MeV/u  $U^{92+}$  on N as a function of the laboratory angle. The approximate RHF wave functions by DZ-STO's [22] have been used for the target atom. All partial waves with  $|\kappa| \leq 10$  have been taken into account in the calculation of the photoelectric cross section.

$L_2$ , and  $L_3$  ( $2s_{1/2}$ ,  $2p_{1/2}$ ,  $2p_{3/2}$ ) is displayed separately. It is found that the peak positions of the angular distributions of  $L$ -REC to the  $2p_{1/2}$  and  $2p_{3/2}$  shells are in the backward direction compared with that to the  $2s_{1/2}$  shell, in contrast to the angular distributions of photoelectric effect [17,23,27]. This is because the REC angular dis-

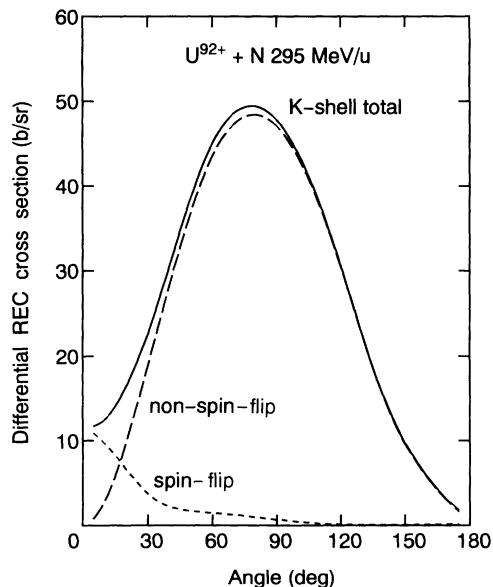


FIG. 5. Calculated differential  $K$ -shell REC cross sections for 295-MeV/u  $U^{92+}$  on N as a function of the laboratory angle. The spin-flip and non-spin-flip contributions of the  $K$  shell are shown separately. The approximate RHF wave functions by DZ-STO's [22] have been used for the target atom. All partial waves with  $|\kappa| \leq 10$  have been taken into account in the calculation of the photoelectric cross section.

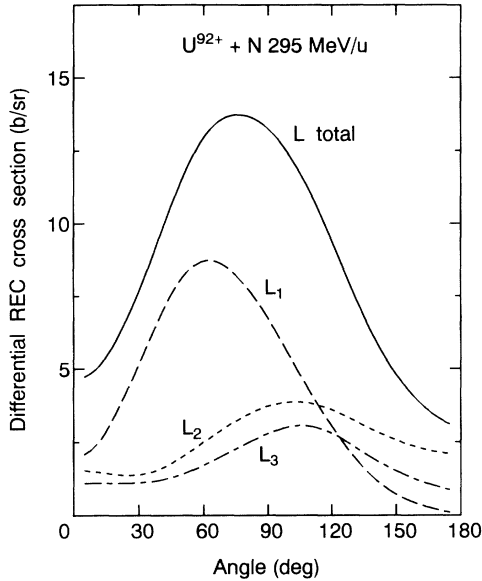


FIG. 6. Calculated differential  $L$ -shell REC cross sections for 295-MeV/u  $U^{92+}$  on N as a function of the laboratory angle. The contributions of the  $L_1$ ,  $L_2$ , and  $L_3$  shells are shown separately. The summed cross section appears again in Fig. 6. The approximate RHF wave functions by DZ-STO's [22] have been used for the target atom. All partial waves with  $|\kappa| \leq 10$  have been taken into account in the calculation of the photoelectric cross section.

tribution at  $\theta'$  corresponds to the photoelectric (or RR) angular distribution at  $\pi - \theta'$ .

### B. Charge and energy dependence of the cross section for radiative recombination

The dependence of REC cross sections on the projectile charge and energy is best represented if we consider radiative recombination (RR), in which the electron is assumed to be at rest in the initial state. Therefore, no target parameters enter. Figure 7 presents a comparison of the exactly calculated cross section (solid line) with the cross section calculated according to the nonrelativistic Stobbe formula [28,29] for radiative electron capture into an empty  $K$  shell given by

$$\sigma_{RR}^{\text{Stobbe}} = \frac{2^8 \pi^2 \alpha}{3} \left( \frac{\nu^3}{1 + \nu^2} \right)^2 \frac{e^{-4\nu \arctan(1/\nu)}}{1 - e^{-2\pi\nu}}, \quad (3.1)$$

where  $\nu = \alpha Z/v$  is the Sommerfeld parameter. Stöhlker [26] has pointed out that for  $K$ -shell RR ( $K$ -RR), the exact relativistic cross section almost coincides with the nonrelativistic Stobbe cross section Eq. (3.1). In Fig. 7, the dotted lines are calculated by assuming the correct relation between the velocity  $v$  and the projectile energy, while the dashed line uses the relation  $E_{\text{kin}} = \frac{1}{2} M_P v^2$ , as if the projectile speed were nonrelativistic. Indeed, we confirm that the completely nonrelativistically calculated cross section for  $K$ -RR is very close to the exact

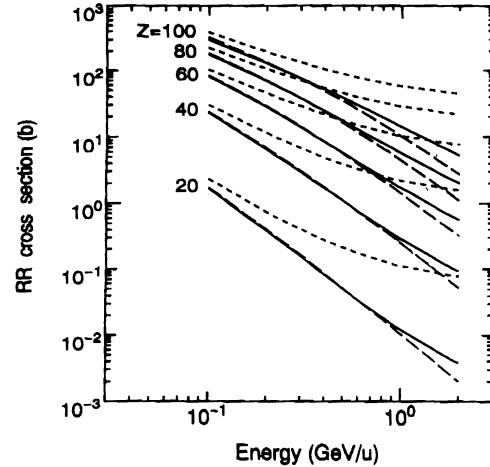


FIG. 7. Energy and charge dependence of the cross section for radiative recombination (in barns) with capture into the projectile  $K$  shell. Solid lines: exact (relativistic) calculated cross sections; dotted lines: Stobbe cross sections, Eq. (3.1), assuming the correct relativistic relation between energy and velocity; dashed lines: Eq. (3.1), but assuming the nonrelativistic relation  $E_{\text{kin}} = \frac{1}{2} M_P v^2$  between energy and velocity. In the relativistic calculations, all partial waves with  $|\kappa| \leq 20$  have been taken into account.

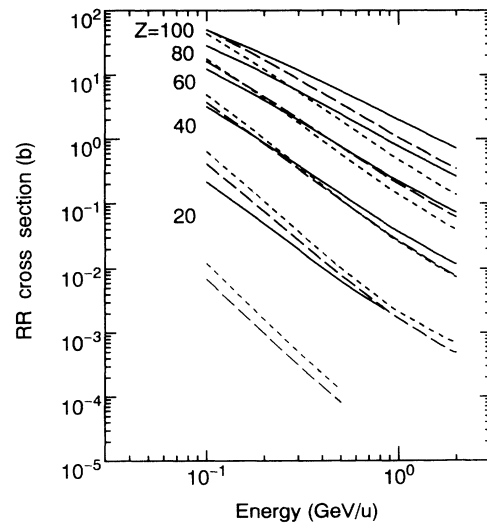


FIG. 8. Energy and charge dependence of the cross sections for radiative recombination (in barns) with capture into the projectile  $L$  shells. All results are obtained from exact relativistic calculations. Solid lines: capture into the  $L_1$  shell; long-dashed lines: capture into the  $L_2$  shell; short-dashed lines: capture into the  $L_3$  shell. The cross sections for  $L_1$  capture are considerably larger than those for the other two shells, so that they appear to group with the next higher charge state. All partial waves with  $|\kappa| \leq 20$  have been taken into account.

relativistic cross section.

This equivalence cannot hold for the differential cross section, which nonrelativistically would be represented by a strict  $\sin^2\theta$  distribution, while in the exact cross sections (see Figs. 4 and 6), considerable deviations from this form occur. One reason is that spin-flip contributions to the cross section, as in Fig. 5, yield nonzero values at forward and backward angles.

In analogy to Fig. 7, we have plotted in Fig. 8 the exact relativistic RR cross sections for capture into the  $L_1$ ,  $L_2$ , and  $L_3$  shells. Here, very clearly, capture into the  $L_1$  shell dominates for all charges and energies.

#### IV. SUMMARY AND CONCLUSIONS

Radiative electron capture dominates over nonradiative capture for high- $Z$  projectiles and low- $Z$  target atoms. Under these conditions, it is well justified to take into account the target atom only through (i) the binding energy of the electron in its initial state and (ii) its bound-state momentum distribution. Beyond this impulse approximation, the present description of REC is rigorous by using exact relativistic bound and continuum Coulomb projectile states in the underlying treatment of the photoelectric effect and by performing an exact convolution with the target momentum distribution. A versatile computer program for REC into arbitrary projectile shells has been developed, which is applicable to a variety of experiments that are currently in progress.

As an illustration, photon spectra and angle-differential cross sections have been calculated. The experimental dependence of  $K$ -REC for the collision system of 197-MeV/u  $\text{Xe}^{54+} + \text{Be}$  is well represented by the calculation. For the collision system of 295-MeV/u  $\text{U}^{92+} + \text{N}$ , Hartree-Fock wave functions reproduce the experimental line shapes of photon spectra very well. The calculations show pronounced deviations from a simple  $\sin^2\theta$  dependence for  $K$ -REC as well as for  $L$ -REC. The importance at forward angles of spin-flip contributions, which cannot be described nonrelativistically, is also demonstrated.

Furthermore, exact relativistic cross sections for radiative recombination have been calculated. The treatment includes capture into the  $K$  shell and into the individual  $L$  subshells for projectile charges between 20 and 100 and energies between 100 MeV/u and 2 GeV/u. These values are useful for simple estimates of total REC cross sections.

#### ACKNOWLEDGMENTS

The authors would like to thank Dr. Y. Kikuchi of Japan Atomic Energy Research Institute (JAERI) for his encouragement during this work. J.E. gratefully acknowledges the cordial hospitality extended to him during his stay at JAERI. He also appreciates useful discussions with Dr. Th. Stöhlker regarding collision systems of experimental interest.

- 
- [1] C.T. Munger and H. Gould, *Phys. Rev. Lett.* **57**, 2927 (1986); C.T. Munger and H. Gould, in *Atomic Physics*, edited by H. Narumi and I. Shimamura (North-Holland, Amsterdam, 1987), Vol. 10, p. 95.
- [2] J. Eichler, *Phys. Rep.* **193**, 165 (1990).
- [3] G. Raisbeck and F. Yiou, *Phys. Rev. Lett.* **4**, 1858 (1971).
- [4] H.W. Schnopper, H. Betz, J.P. Devaille, K. Kalata, A.R. Sohval, K.W. Jones, and H.E. Wegner, *Phys. Rev. Lett.* **29**, 898 (1972).
- [5] P. Kienle, M. Kleber, B. Povh, R.M. Diamond, F.S. Stephens, E. Grosse, M.R. Maier, and D. Proetel, *Phys. Rev. Lett.* **31**, 1099 (1973).
- [6] J.S. Briggs and K. Dettmann, *Phys. Rev. Lett.* **33**, 1123 (1974); J.S. Briggs and K. Dettmann, *J. Phys. B* **10**, 1113 (1977).
- [7] M. Kleber and D.H. Jakubassa, *Nucl. Phys. A* **252**, 152 (1975).
- [8] R. Shakeshaft and L. Spruch, *Phys. Rev. Lett.* **38**, 175 (1977).
- [9] R. Schulé, H. Schmidt-Böcking, and I. Tserruya, *J. Phys. B* **10**, 889 (1977); J.A. Tanis and S.M. Shafroth, *Phys. Rev. Lett.* **40**, 1174 (1978).
- [10] E. Spindler, Ph.D. thesis, München University, 1979; E. Spindler, H.-D. Betz, and F. Bell, *Phys. Rev. Lett.* **42**, 832 (1979).
- [11] M. Gorriz, J.S. Briggs, and S. Alston, *J. Phys. B* **16**, L665 (1983); D.H. Jakubassa-Amundsen, R. Hoeppler, and H.-D. Betz, *ibid.* **17**, 3943 (1984); D.H. Jakubassa-Amundsen, *ibid.* **20**, 325 (1987); M.C. Pacher, A.D. Gonzales, and J.E. Miraglia, *Phys. Rev. A* **35**, 4108 (1987).
- [12] H. Tawara, P. Richard, and K. Kawatsura, *Phys. Rev. A* **26**, 154 (1982).
- [13] R. Anholt, S.A. Andriamonje, E. Morenzoni, Ch. Stoller, J.D. Molitoris, W.E. Meyerhof, H. Bowman, J.-S. Xu, Z.-Z. Xu, J.O. Rasmussen, and D.H.H. Hoffmann, *Phys. Rev. Lett.* **53**, 234 (1984).
- [14] W.E. Meyerhof, R. Anholt, J. Eichler, H. Gould, Ch. Munger, J. Alonso, P. Thieberger, and H.E. Wegner, *Phys. Rev. A* **32**, 3291 (1985); R. Anholt, Ch. Stoller, J.D. Molitoris, D.W. Spooner, E. Morenzoni, S.A. Andriamonje, W.E. Meyerhof, H. Bowman, J.-S. Xu, Z.-Z. Xu, J.O. Rasmussen, and D.H.H. Hoffmann, *ibid.* **33**, 2270 (1986).
- [15] K.I. Hino and T. Watanabe, *Phys. Rev. A* **36**, 581 (1987); **39**, 3373 (1989).
- [16] F. Sauter, *Ann. Phys. (Leipzig)* **9**, 217 (1931); **11**, 454 (1931); U. Fano, K.W. McVoy, and J.R. Albers, *Phys. Rev.* **116**, 1147 (1959); R.H. Pratt, R.D. Levee, R.L. Pexton, and W. Aron, *ibid.* **134**, A898 (1964); **134**, A916 (1964).
- [17] R.H. Pratt, A. Ron, and H.K. Tseng, *Rev. Mod. Phys.* **45**, 273 (1973). A misprint in the normalization, Eq. (4.2.22), has been corrected. The expression  $[(E \pm 1)^{1/2}/2E]$  should be replaced with  $[(E \pm 1)/2E]^{1/2}$ . In this case, agreement with [19,23] is obtained.
- [18] B.C.H. Nagel, *Ark. Fysi.* **18**, 1 (1960); M. Gavrilu, *Phys.*

- Rev. **113**, 514 (1959); Nuovo Cimento **15**, 691 (1960).
- [19] S. Hultberg, B. Nagel, and P. Olsson, Ark. Fys. **38**, 1 (1967); J.H. Scofield, University of California Report No. UCRL-51326, 1973 (unpublished).
- [20] B. Müller, J. Rafelski, and W. Greiner, Nuovo Cimento A **18**, 551 (1973).
- [21] M.E. Rose, *Relativistic Electron Theory* (Wiley, New York, 1961).
- [22] E. Clementi and C. Roetti, At. Data Nucl. Data Tables **14**, 177 (1974).
- [23] W.R. Alling and W.R. Johnson, Phys. Rev. **139**, A1050 (1965).
- [24] Th. Stöhlker, C. Kozhuharov, A.E. Livingston, P.H. Mokler, and A. Warczak, Z. Phys. D **23**, 121 (1992).
- [25] Th. Stöhlker, P.H. Mokler, T. Kandler, C. Kozhuharov, R. Moshhammer, P. Rymuza, Z. Stachura, A. Warczak, K. Beckert, F. Bosch, H. Eickhoff, B. Franzke, M. Jung, O. Klepper, F. Nolden, H. Reich, P. Spädtke, and M. Steck, in *Proceedings of the 18th International Conference on the Physics of Electronic and Atomic Collisions, Aarhus, 1993*, edited by T. Andersen, B. Fastrup, F. Folkmann, and H. Knudsen (Aarhus University, Aarhus, 1993), p. 617.
- [26] Th. Stöhlker (private communication).
- [27] H. Brysk and C.D. Zerby, Phys. Rev. **171**, 292 (1968).
- [28] M. Stobbe, Ann. Phys. (Leipzig) **7**, 661 (1930).
- [29] H.A. Bethe and E.E. Salpeter, *Quantum Mechanics of One- and Two Electron Atoms* (Springer-Verlag, Berlin, 1957).